MQ232, A Snake Toxin Derivative for Treatment of Hyponatremia and Polycystic Kidney Diseases

Goran Stanajic-Petrovic, Mathilde Keck, Peggy Barbe, Apolline Urman, Evelyne Correia, Pierre Isnard, Jean-Paul Duong van Huyen, Khawla Chmeis, Sékou Siramakan Diarra, Stefano Palea, et al.

MQ232, A Snake Toxin Derivative for Treatment of Hyponatremia and Polycystic Kidney Diseases

Goran Stanajic-Petrovic[1,2], Mathilde Keck[1], Peggy Barbe[1], Apolline Urman[1,2], Evelyne Correia[1], Pierre Isnard[3], Jean-Paul Duong Van Huyen[3], Khawla Chmeis[2], Sékou Siramakan Diarra[4], Stefano Palea[4], Frederic Theodoro[1], Anvi-Laëtitia Nguyen[1], Florence Castelli[1], Alain Pruvost[1], Wenchao Zhao[5], Christiane Mendre[6], Bernard Mouillac[6], Frank Bienaimé[7], Philippe Robin[1], Pascal Kessler[1], Catherine Llorens-Cortes[1], Denis Servent[1], Hervé Nozach[1], Bernard Maillère[1], Dong Guo[5], Charles Truillet[2]*, Nicolas Gilles[1]*

1 : Université Paris Saclay, CEA, Département Médicaments et Technologies pour la Santé (DMTS), SIMoS, 91191 Gif-sur-Yvette, France
2 : Université Paris-Saclay, CEA, CNRS, Inserm, BioMaps, Orsay, 91401, France
3 : Anatomie et Cytologie Pathologiques, CHU Necker-Enfants Malades, 149 rue de Sèvres, 75015 Paris, France
4 : Humana Biosciences, Prologue Biotech, 516 Rue Pierre et Marie Curie, 31670, Labège, France
5: Jiangsu Key Laboratory of New Drug Research and Clinical Pharmacy, Xuzhou Medical University, Jiangsu, China
6: IGF, Univ. Montpellier, CNRS, INSERM, Montpellier, France
7: Département Croissance et Signalisation, Institut Necker Enfants Malades, INSERM U1151, CNRS UMR 8253, Université de Paris Cité, Paris, France ; Service d'Explorations Fonctionnelles, Hôpital Necker Enfants Malades, Assistance Publique-Hôpitaux de Paris
*: corresponding authors.

Corresponding authors:
Dr. Charles Truillet, Université Paris-Saclay, CEA, CNRS, Inserm, BioMaps, Orsay, 91401, France
charles.truillet@universite-paris-saclay.fr

Dr. Nicolas Gilles, Université Paris Saclay, CEA, Département Médicaments et Technologies pour la Santé (DMTS), SIMoS, 91191 Gif-sur-Yvette, France. 33-169086547, nicolas.gilles@cea.fr

ABSTRACT

Background: Vaptans were developed at the end of the previous century as V2R antagonists. Tolvaptan is the most prescribed vaptan for hyponatremia and the autosomal polycystic kidney disease (ADPKD). However, its use is not as widespread as it should be due to price issues, a narrow therapeutic window and some side effects. With the aim of discovering new efficient and safer V2R antagonists, we screened animal venoms and identified several interesting peptide toxins. Among them, MQ1 displayed such unique biological properties in that regard that it was the starting point for the development of a potential drug candidate.

Methods: Human T-cell assays and bioinformatics was used to mitigate MQ1 immunogenicity risk. The MQ232 biodistribution in mice was done by positron emission tomography (PET). Pharmacodynamics, pharmacokinetics, acute and chronic toxicity tests were performed on control rats. A rat experimental model of dDAVP-induced hyponatremia, an *ex vivo* mice model of renal cysts and a mice orthologous model of ADPKD were used to validate MQ232 efficacy in these pathologies.

Results: Three mutations were introduced in MQ1 to mitigate its immunogenicity risk. A fourth gain-of-function mutation was added to generate MQ232. MQ232's safety was demonstrated by a first toxic dose as high as 3,000 nmol/kg and a strong kidney organ selectivity by PET imaging, while showing almost no interaction with the liver. MQ232's efficacy was first demonstrated with an effective dose of 3 nmol/kg in a hyponatremic model, and then in polycystic kidney models on which MQ232 significantly reduced cyst growth.

Conclusions: We demonstrated, employing diverse translational techniques and minimizing animal use, MQ232's safety and efficacy in several rodent models of hyponatremia and ADPKD.

INTRODUCTION

The vasopressin type 2 receptor (V2R) is expressed in the distal convoluted tubule and collecting ducts of the kidneys and regulates body fluid homeostasis[1–3]. Its blockade by vaptans is an efficient and validated therapeutic strategy for hyponatremia[4–8] and autosomal dominant polycystic kidney disease (ADPKD)[9–13]. Hyponatremia is a prevalent electrolyte disorder characterized by a plasma sodium concentration below 135 mmol/l. It can be induced by an inappropriate secretion of anti-diuretic hormone (SIADH)[14–18], congestive heart failure[19–21] especially when patients are resistant to diuretics[22,23] and also cirrhosis[24–27], mainly associated with refractory ascites[28–32]. Finally, a large proportion of hyponatremic patients are not treated correctly[14] while hyponatremia is associated with an increase in mortality risk[33–36] and increased hospital costs and readmission rates[37–39]. The market-available vaptans, the conivaptan (Vaprisol®, Cumberland Pharmaceuticals, U.S.A), mozavaptan (Physuline®, Otsuka, Japan) and tolvaptan (Samsca®, Otsuka Pharma), this last being by far the most used, have limited usage primarily due to their hepatotoxicity, drug-drug interactions and the challenge for physicians to establish an appropriate, patient-tailored dosage[40].

Polycystic kidney diseases (PKDs) are a group of ciliopathies causing significant renal failure in children and adults with no curative treatments[41]. The autosomal dominant polycystic kidney disease (ADPKD) is induced by mutations in either the *Pkd1* or *Pkd2* gene encoding multimembrane-spanning polycystin-1 and polycystin-2, respectively[42–45]. The recessive form of PKD, the autosomal recessive polycystic kidney disease (ARPKD), is due to mutations in the *PKHD1* gene encoding for the fibrocystin[46,47]. It is suggested that increased cyclic AMP production has a critical role in the formation and expansion of cysts[48–50]. PKDs initiate a ceaseless formation and growth of fluid-filled cysts leading to the loss of kidney function. Tolvaptan is the only approved drug for adult ADPKD patients with fast deterioration of their kidney functions[51–55]. Patients are often treated for hypertension by liver-metabolized molecules, making drug-drug interactions difficult to deal with. Emerging studies reported debates among nephrologists with concerns regarding tolvaptan's narrow therapeutic window[56,57]. ARPKD on its own is still an orphan disease.

We screened animal toxins for peptides active on human V2R to address these V2R-related pathologies by vaptan-unrelated molecules with the hope of generating a safe and efficient drug candidate. Animal toxins have evolved for millions of years, allowing them to acquire potent biological activities. Toxins are generally active at very low doses and design to quickly reach their target *in vivo*[58–62]. To broaden efficacy while minimizing side effects, we identified nine next-generation V2R antagonists from African mamba snake venoms[63,64]. Among them, MQ1 emerged as one of the most potent and selective V2R antagonist known to date[63]. To harness the interesting properties of this natural peptide and develop it into a promising drug candidate, we undertook an engineering process resulting in the evolution from MQ1 to the enhanced form MQ232 being fully investigated here.

METHODS

Information on commercially available kits, buffers, and chemistry used in the study and other methodical details including methods relevant to Supplemental Results are provided in Supplemental Materials.

Prediction and identification of CD4 T cell epitopes in humans

Putative immunogenic sequences (CD4 T cell epitopes) were predicted using netMHCIIpan3.2 algorithm[65]. T cell epitopes were identified by generation of human T cell lines and assessment of their peptide specificity by IFN-γ ELISPOT using overlapping peptides[66].

Chemistry

MQs were produced by solid-phase-peptide-synthesis, deprotected, purified and folded as described[64]. Deferoxamine-(DFO)-MQ232 was radiolabeled with ^{89}Zr (90 MBq) at 37 °C for 60 min. Radiochemical yield and purity were determined using instant thin-layer chromatography and further confirmed by radio-HPLC. The final specific activity was determined to be 28.6 ± 6.2 MBq/ng.

In vitro pharmacology

Binding experiments were performed using 1 nM [^{3}H]AVP in a 100-µL reaction mixture[64]. Data were fitted to a one-site inhibition mass action curve using GraphPad Prism (San Diego, USA) and IC_{50} values were converted to K_i using 1.1 nM as [^{3}H]AVP Kd.

cAMP cell-based assay. $5x10^3$ CHO-hV2R cell line/well were incubated 30 min at 37°C with AVP DMEM solutions in the presence of MQs. Reaction was stopped with cAMP Gs dynamic kit HTRF from Cisbio[63].

V2-β-arrestin interaction BRET assay. $75x10^3$ electroporated tsA cells/well with human V2R-RLuc and β-arrestin-1-YFP were incubated with Krebs/Coelenterazine H before addition of AVP/CoH solutions in the presence of MQs. EC_{50} values were calculated from Kinetics BRET[63].

V2R internalization assay by DERET. $9x10^4$ electroporated HEK Magik cells/well with Flag-ST-human V2R were labeled with SNAP-Lumi4-Tb and incubated with AVP in Krebs/BSA 0,2%/Fluorescein in the presence of MQs. Human V2R surface expression level was determined by measuring SNAP-Lumi4-Tb fluorescence at indicated times and area under kinetics curve to obtain related EC_{50} values from dose-response curves.

MAP kinase phosphorylation. $5x10^4$ Myc-hV2R HEK cell/well were starved and stimulated with AVP in the presence of MQs. AVP-stimulated MAPK phosphorylation was evaluated using the Cellul'erk kit from Cisbio Bioassays (Codolet, France)[63].

Mini G protein recruitment assays under vasopressin stimulation were performed on 10^6 HEK293T cells transiently co-expressing the human V1aR or human V1bR or human V2R, plus the cognate mini Gq protein fused to NanoLuc (mini-Gq for human V1a/bR and mini-Gs for human V2R) plus the membrane anchored venus-KRas protein. Cells were stimulated in the presence of AVP and MQ232 or tolvaptan at various concentrations. BRET recordings were performed in the presence of the NanoLuc substrate furimazine. Values at plateaus of the kinetic curves were used to obtain the dose-response curves and the IC_{50} values.

Pharmacodynamics, pharmacokinetics, and safety analysis

For pharmacodynamic experiments, rats were injected with MQ232 before urine collection in metabolic cages.

For the pharmacokinetic experiments, blood samples were taken at various times and analyzed by MS. Plasma plus the internal standard (MQ232-A39K) was treated by Solid Phase

Extraction, reduced and alkylated and analyzed with the LC-MS/MS Nexera (Shimadzu, France) coupled to MS on Quantum Ultra™ (ThermoFisherScientific, France) for the quantification of MQ232.
For the safety experiments, MQ232 was s.c. administered acutely or chronically for 21 days before urine, plasma, and organs analysis.

PET imaging
[^{89}Zr]Zr-DFO-MQ232 was i.v. administered through tail vein on anesthetized mice and imaged with a Siemens Inveon (Siemens, USA) by small-animal-adapted PET/CT sessions. Images were corrected for attenuation using a 20-minute computed tomography (CT) scan performed consecutively to the PET, reconstructed using a 3D OSEM iterative algorithm and data extraction done using PMOD for signal intensity for pharmacokinetic parameter determination.

Pathological rodent model experiments
For the SIADH model of hyponatremia, rats were infused with 10 ng/h of dDAVP. Natremia was measured over time[67].
Mice embryonic kidneys were cultured[68,69] and treated six days with MQ232. The cystic index was quantified by analyzing the ratio of cyst area to the total area of the kidney section using ImageJ (Version 1.53c). MQ232 or vehicle were s.c. administered to the WT (Pkd1+/+;Ksp-Cre) and ADPKD (Pkd1flox/flox;Ksp-Cre)[70] mice from day 6 to day 12. Kidneys were harvested to calculate the total kidney to body weight ratio. Kidneys were fixed for histological examination.

***In vivo* experiment authorizations**
All animal procedures were performed in accordance for Care and Use of Laboratory Animals of the Directive 2010/63/EU of the European Parliament. These procedures were approved by local Ethics Committee and obtained the authorizations.

Data processing and statistical analysis
Data are shown as means ± standard error of the mean. Normality was assessed using the d'Agostino-Pearson test, comparisons between two groups using the unpaired Student's t test, comparisons between more than two groups using the Kruskal–Wallis test followed by Dunn's test. ANOVA multiple factors followed by Tukey's test was used to compare repeated measurements. Statistical analyses were performed using GraphPad Prism 9.5.1 software.

RESULTS

Engineering MQ232

The immunogenicity of protein therapeutics may be an issue resulting in reduced efficacy, anaphylaxis and occasionally life-threatening autoimmunity[71]. European and American regulatory agencies recognize limited predictive value of animal models for human immunogenicity and recommend alternative approaches for risk evaluation. Natural MQ1[63] being a non-human peptide, we employed human T-cell assays to evaluate its immunogenicity risk and bioinformatics tools to mitigate it. CD4 T-cells specific for MQ1 were derived from human blood samples and their peptide specificity were assessed by stimulating them with 15-mer peptides overlapping by 12 amino acids encompassing the MQ1 sequence (Figure 1A)[72,73]. T-cell lines were found to be specific for peptides P6, P7, P8 and to a lesser extent for P1, P14 and P15 (Figure 1B). The bioinformatics tool NetMHC 3.2 (Jensen[74]) identified as major anchoring amino acids for HLA-DR molecules the F20 (P6-P7), Y21 (P6-P8) and F44 (P14-P15). However, we never succeeded in the substitution of these residues due to their critical role in MQ1 structure. We thus mitigated the immunogenicity of peptides P1, P14, and P15 by substituting the putative HLA anchor F4 with glycine and I48 with glutamic acid, resulting in MQ211 (Figure 1C, Supplemental Figure 1). MQ211 kept the MQ1's affinity for human V2R and showed lower HLA-binding score. In the P6-P8 zone, T27 was successfully substituted by an aspartic acid (MQ228). MQ228 preserves the MQ1's affinity but combines a null HLA-binding score. In addition to these 3 mutations which reduce the risk of immunogenicity, we added the K39A gain-of-function substitution that was previously identified[64]. Added to MQ228, the resulting MQ232 (Supplemental Figure 1) showed a sub-nanomolar affinity and HLA-DR binding score close to zero (Figure 1C). Through computational simulations and iterative experimental design, natural MQ1 properties were optimized to enhance its safety and efficacy thanks to extensive efforts in preserving the toxin's structure.

Pharmacological characterization of MQ232

MQ1[63,64,67] displays binding affinities of 4.56 nM (pK_i 8.37 ± 0.07) for the human V2R using tritiated AVP as radioligand (Figure 2A). MQ232 displays binding affinities of 0.37 nM (pK_i 9.60 ± 0.19) for the human V2R and 1.89 nM (pK_i 8.73 ± 0.04) for the rat V2R (Figure 2A, Supplemental Table 1). MQ232 consistently outperforms MQ1 in its ability to antagonize the three AVP-induced V2R signaling pathways linked to the cAMP production, the β-arrestin-1 recruitment and the MAP kinase phosphorylation. In addition, both peptides block the AVP-induced Flag-Snap-hV2R internalization (Figure 2B-E, Supplemental Table 2, Supplemental Figure 2). Like MQ1, MQ232 displays a selectivity factor higher than 100 times in the favor of human V2R *vs* human V1aR and human V1bR (Supplemental Figure 3). Control Sprague-Dawley rats spontaneously urinated on average 1.79 mL/h/kg body weight (BW) with an osmolality of 1475 mOsm/kg H_2O, corresponding to an electrolyte excretion of 60 Osm/d/kg BW, without sex-linked differences. Acute subcutaneous (s.c.) injections of MQ232 with doses from 1 to 3,000 nmol/kg BW, dose-dependently increased 24-h aquaresis from 2.6 to 12.0 mL/h/kg BW in parallel with decrease in osmolality (Figure 2F, Supplemental Table 3). No significant loss of electrolytes was noticed, no perturbation of any of the 32 blood or urine measured parameters could be detected (Supplemental Table 3) and no histologic sign of toxicity on the 6 examined organs could be seen (Supplemental Figure 4, Supplemental Table 4). The unique toxicity sign was detected on only 1 rat out of the 6 injected with the highest dose of 3,000 nmol/kg. This rat presented an apathetic behavior, a 24 % weight loss and an enlarged right kidney (Supplemental information 1, Supplemental Figure 5). Aquaresis was maximal between the first and second hour with a maximal aquaresis around 50 mL/h/kg BW

and exhibited a mono-exponentially decrease with a $T_{1/2}$ of 1.33 ± 0.13 h (0.7-1.7 h, Figure 2G, Supplemental Table 5). Pharmacokinetics parameters of MQ232 were determined after intravenous (i.v., Supplemental Figure 6) and intraperitoneal (i.p., Supplemental Figure 7) injection of 30 nmol/kg BW (Figure 2H, Supplemental Table 6-7). A mono-compartmental distribution was observed with a $T_{1/2}$ of 0.96 and 1.1 h and total areas under curve (AUCtot) of 0.47 and 0.52 µg/mL*h respectively, giving a peptide biodistribution of 100% by i.p. *vs* i.v. route (Figure 2H, Supplemental Table 8). Intraperitoneal injection of 300 nmol/kg BW of MQ232 (Supplemental Figure 8) displayed a 10-time higher AUCtot of 5.9 µg/mL*h and a $T_{1/2}$ of 2.1 h, demonstrating a good linearity between injected doses and circulating concentrations of MQ232. MQ232 distributes with a small apparent volume ranging from 450 to 780 ml/kg, its clearance being between 6.34 and 7.53 ml/min/kg. Finally, there is a good linear relationship between aquaresis and MQ232 plasma concentration (R^2= 0.91, Figure 2I, Supplemental Table 9). Aquaresis of rats continuously infused for 21 days with 0, 0.5 or 5 nmol/h/kg BW of MQ232 raised from 1.12 ml/h/kg BW (0 nmol/kg/h, control) to 4.09 (0.5 nmol/kg/h) and 14.40 ml/h/kg BW (5 nmol/kg/h, Supplemental Table 10). For the dose of 5 nmol/h/kg BW, MQ232 plasma concentrations ranged between 11.3 and 15.2 nM. Those aquaresis raises were associated with a urine osmolality decrease without electrolyte loss. No modification in the 34 urine and blood biochemical parameters nor in the 6 observed organs, including liver, were observed (Supplemental information 2, Supplemental Figure 9). The expression of Lipocalin 2 (LCN2), a highly sensitive tubule injury marker remained undetectable in the collecting ducts of the rats treated for 21 days with 0 or 5 nmol/h/kg of MQ232 (supplemental Figure 10).

MQ232 pharmacokinetic and tissue distribution derived from PET imaging in control mice

Positron Emission Tomography (PET) is a powerful imaging modality thanks to its high sensitivity and *in vivo* dynamic imaging capabilities. Deferoxamine (DFO) is the most widely used chelator for ^{89}Zr labeling[75]. A DBCO-derived DFO was cyclo-added to the azido-MQ232 to generate the DFO-MQ232 (Figure 3A, Supplemental Figure 1). [^{91}Zr]Zr-DFO-MQ232 displays affinities of 0.82 (pK_i = 9.12 ± 0.08) and 2.47 nM (pK_i = 8.64 ± 0.08) for human V2R and rat V2R respectively (Figure 2A, Supplemental Table 1), demonstrating the minimal influence of this modification. The radiolabeling yield of DFO-MQ232 with ^{89}Zr demonstrated high efficiency, exceeding 95% (Figure 3B). Capitalizing on PET's significant sensitivity, we administered [^{89}Zr]Zr-DFO-MQ232 at a low dose of 40 ± 5 µg (4.28 ± 0.18 MBq) into control mice. Notably, there were no observed toxic effects post-injection, emphasizing the ability to achieve distinct distribution without adverse impacts on the biological milieu. The dynamic acquisition, PET reconstruction as well as the fusion of PET with CT images allowed the determination of MQ232's whole-body behavior overtime (Figure 3C). 62 ± 8% of the injected [^{89}Zr]Zr-DFO-MQ232 accumulated favorably in the kidney during the first hour. Gallbladder, colon and liver respectively accumulated 9 ± 0.4, 6 ± 1 and 5 ± 0.5 % of the injected dose (Figure 3D, Supplemental Table 13). It is worth noting that the liver signal is classically overestimated due to the transmetalation occurring between Zr and Fe ions[76]. No other organs were significantly labelled except the bladder, as the kidney is also the metabolizing organ for [^{89}Zr]Zr-DFO-MQ232. The analysis of MQ232's uptake within the blood pool allows specific pharmacokinetic parameters extraction (Figure 3E, Supplemental Table 4). A factor of almost 8 was obtained between the blood and kidney AUC in favor of the latter (Figure 3F), showing a high plasmatic clearance and a strong affinity of the radiotracer for the kidneys. We used a one-compartment open model to fit the image-derived blood activity, enabling the determination of MQ232 $t_{1/2}$ to be 27 ± 4 (16 to 40) min (Figure 3F, Supplemental Table 14), in accordance with the one determined in rats[77].

MQ232's efficacy in experimental rodent models of hyponatremia and PKDs

The rat model of SIAD was obtained by s.c. infusion of 10 ng/h of dDAVP and water gavage from D0 to D4[78,79]. In vehicle-treated rats, plasma sodium concentration ([Na^+]) lowered from 141.7 ± 0.63 to 124.5 ± 4.17 mM between D0 and D4 (Figure 4A, Supplemental Table 15). MQ232 and tolvaptan were administrated at day 2, 3 and 4. Tolvaptan (22 µmol/kg BW p.o.) partially restored natremia levels at D4 only (plasma [Na^+] = 137.6 mM) and with a plasma [Na^+] rise of 4.8 mM/d. MQ232 (3.1 nmol/kg BW s.c.) restored natremia from D3 (plasma [Na^+] = 142.7 mM, Figure 4A, Supplemental Table 15) and with plasma [Na^+] rises between 6.9 mM/d and 7.5 mM/d. The 9.6 nmol/kg BW s.c. MQ232 dose gave no additional effect. Apart from a moderate weight loss due to the highly stressful model for rats, no toxicity signs were observed (Supplemental Table 16).

We evaluated MQ232 activities *ex vivo* on an embryonic kidney developing cyst under 8-Br-cAMP stimulation[69,70]. The cystogenesis effect (Figure 4B, Supplemental Table 17) was significantly inhibited by 1 µM of MQ232 as the ratio cyst area on total kidney area was reduced from 37% to 26% (Figure 4C). Next, we used kidney-selective *Pkd1* knockout mice (*Pkd1*$^{flox/flox}$*;Ksp-Cre*) orthologous model of ADPKD[69,70]. Compared with the vehicle-treated group and after 12 days of treatment, MQ232 concentration-dependently slowed kidney enlargement (Figure 4D, Supplemental Table 18). Indeed, kidney index (KW/BW, Figure 4E) diminished from 20% to 18% and to 13% with 0.1 and 1 µmol/d/kg BW of MQ232, respectively.

DISCUSSION

In this work, we use a large array of techniques to investigate the efficacy and safety of a new class of aquaretic agents, led by MQ232. This peptide derived from a natural snake toxin called MQ1 displays much lower risk of immunogenicity by *in silico* evaluation associated with a 12-fold higher affinity for the human V2R. MQ232's safety is favorable with a maximum tolerate dose in rat of 1,000 nmol/kg combined with an *in vivo* selectivity for the kidney organ. It appears to be predominantly eliminated through the kidneys, this being supported by its creatinine-like high clearance with low reabsorbtion[80,81] and peptide nature. Lastly, its minimal uptake by the liver allows the anticipation of a reduced drug-drug interaction probability, particularly appreciated in the case of polymedicated patients.

In healthy rats, MQ232 increases aquaresis starting from the dose of 3 nmol/kg. This dose was sufficient to restore natremia in our experimental model of hyponatremia. The use of aquaretic agents stands out as the most effective strategy for normalizing natremia in cases of euvolemic and hypervolemic hyponatremia, particularly when it is caused by excessive AVP production. Interestingly, MQ232 quickly restores natremia at a patient safety compatible rate. It is indeed crucial for hyponatremic patients to i) receive prompt medical attention to minimize the detrimental effects associated with low plasma sodium concentrations, ii) control the natremia's increase rate, aiming for less than 12 mM/d to prevent osmotic demyelination syndrome[83–85], iii) avoid hypernatremia[14]. MQ232 completely respected these conditions. The parenteral administration of MQ232 coupled with its rapid action and swift elimination from the rat body could confer a substantial advantage for emergency physicians involved in natremia rescue. Additionally, MQ232 could offer additional safety benefits with a therapeutic window in rat being over 300 times higher than the effective dose and associated with a strong correlation between urine output and plasma MQ232 concentration. These qualities anticipate a wide safety

margin and reduced adverse effects' likelihood in the case of accurate dosage adjustments and monitoring.
Polycystic kidney diseases, whether dominant or recessive, are still incurable and only V2R blockade has been shown to be truly effective in humans. MQ232 showed a dose-dependent efficacy on an *ex vivo* experimental model and on an orthologous mice model of ADPKD. We have thus validated the use of MQ232 for these pathologies even if these initial findings warrant validation through additional toxicity studies, encompassing both males and females and employing models that exhibit a gradual cyst progression, mirroring the natural history of ADPKD. The parenteral administration of MQ232 may be an issue for ADPKD patients. The use of a pump like for insulin or a slow-release formulation like for GLP1 analogs, may provide a more convenient solution.

Nature is an incredible source of drug candidates[86] and animal venoms a reservoir of millions of peptides selected by evolution for high efficiencies at very low doses. When a venomous animal bites a prey or a predator, it cannot control neither the real quantity injected, nor the exact administration route of its venom[87]. Thus, toxins must act quickly regardless of the injection site. This swift effect is crucial to prevent the prey from escaping or the predator from killing the venomous animal. MQ232 possesses all of these interesting qualities. It acts very quickly on aqueous diuresis after injection, its efficacy at triggering it is equal between i.v. or i.p. injection routes and the first active dose is as low as 3 nmol/kg BW.
MQ232 showed compatible efficacy for *in vivo* V2R imaging by PET. This tool holds the potential to introduce a novel approach for categorizing ADPKD patients. Kidney size is currently evaluated by echography and/or MRI technics[51], but gives no information on the density of treatment-accessible V2R. The response to tolvaptan varies among individuals with ADPKD, some patients experience a beneficial response while others may show no significant improvement. Individual factors, such as genetic variations and disease severity contribute to the variability of responses to tolvaptan.V2R expression's level in ADPKD patients may also potentially be related to their response variability to this drug. PET-compatible, MQ232-based imaging agents may offer, after validation, a promising pathway to investigate the role of V2R binding sites' density in treatment outcomes. By studying the relationship between V2R expression and treatment response, physicians may gain valuable insights on the mechanisms underlying inter-patient variations in drug efficacy.
In conclusion, MQ232, derived from a natural peptide, is a new class of biological V2R antagonist and a promising drug candidate for hyponatremia and ADPKD.

ACKNOWLEDGMENTS

We thank the staff members of *Plateforme d'Histologie et de morphologie du petit animal* of Necker (Paris, France). Humana Biosciences was sponsored by the CEA. Dr. Nicolas Gilles co-founded the startup V4Cure (patent N°EP4171607A1).

TABLE OF CONTENTS FOR THE SUPPLEMENTAL MATERIAL

Supplemental Methods
Supplemental Figure 1. Chemical synthesis of MQs.
Supplemental Figure 2. Functional characterization of MQ1 and MQ232.
Supplemental Figure 3. Functional characterization of MQ232 on hV1aR, hV1bR and hV2R.
Supplemental Figure 4. Pathological study of rat organs from the acute protocol
Supplemental Figure 5. Necroscopy of the female rat (n° 91109).
Supplemental Figure 6. MQ232 blood concentration evolution with time after acute i.v. injection of 30 nmol/kg.
Supplemental Figure 7. MQ232 blood concentration evolution with time after acute i.p. injection of 30 nmol/kg.
Supplemental Figure 8. MQ232 blood concentration evolution with time after acute i.p. injection of 300 nmol/kg.
Supplemental Figure 9. Pathological study of rat organs from the chronic protocol.
Supplemental Figure 10. MQ232 does not increase the expression of the injury marker Lipocalin 2 (Lcn2) in chief collecting duct cells.
Supplemental Figure 11. Pathological study showing inconspicuous mast cell hyperplasia.
Supplemental Table 1. Binding values of MQ232 and [91Zr]Zr-DFO-MQ232 on human and rat V2R.
Supplemental Table 2. Inhibition of various V2R signaling pathways by MQ232.
Supplemental Table 3. Blood and urine analysis of rats after acute injection with MQ232.
Supplemental Table 4. Rat organ histology after acute s.c. injection of various doses of MQ232.
Supplemental Table 5. Pharmacodynamics (s.c. route) and determination of the half-life time of MQ232 on rats.
Supplemental Table 6. Pharmacokinetics parameters after i.v. administration of 30 nmol/kg of MQ232 in rats.
Supplemental Table 7. Pharmacokinetics parameters after i.p. administration of 30 nmol/kg of MQ232 on rats.
Supplemental Table 8. Pharmacokinetics parameters after i.v. administration of 300 nmol/kg of MQ232 on rats.
Supplemental Table 9. Summary of the MQ232 pharmacokinetics parameters.
Supplemental Table 10. Blood and urine analysis of rats infused with MQ232.
Supplemental Table 11. Blood MQ232 concentration during infusion of 5 nmol/kg/h BW.
Supplemental Table 12. Rat organ histology after chronic infusion of various doses of MQ232.
Supplemental table 13. Averaged PET-obtained activities, by organ
Supplemental Table 14. Corrected time-activity curve data for each mouse used for plasma half-life determination.
Supplemental Table 15. Mean and SEM values for natremia (mmol/l) in hyponatremic rat model treated with MQ232 or tolvaptan.
Supplemental table 16. Mean and SEM values for body weight (BW, g) in hyponatremic rat model treated with MQ232 or tolvaptan.
Supplemental Table 17. Kidney index of the ex vivo mouse model of PKD treated with MQ232 (1 μM, n = 8) or vehicle (NaCl 0.9%, n = 6) on day 6.
Supplemental Table 18. Body and kidney weight of the Pkd1 knockout male mice (Pkd1flox/flox;Ksp-Cre) i.p. injected for 12 days with MQ232 (1 μmol/d/kg BW) or vehicle (NaCl 0.9%).
Supplemental Information 1. Acute safety
Supplemental Information 2. Chronic safety

REFERENCES

1. Sparapani S, Millet-Boureima C, Oliver J, Mu K, Hadavi P, Kalostian T, et al.: The Biology of Vasopressin. *Biomedicines* [Internet] 9: 89, 2021
2. Mutig K, Paliege A, Kahl T, Jöns T, Müller-Esterl W, Bachmann S: Vasopressin V2 receptor expression along rat, mouse, and human renal epithelia with focus on TAL. *Am J Physiol Renal Physiol* [Internet] 293: F1166-77, 2007
3. Park F, Mattson DL, Skelton MM, Cowley AW: Localization of the vasopressin V1a and V2 receptors within the renal cortical and medullary circulation. *Am J Physiol* 273: R243-51, 1997
4. Adrogué HJ, Tucker BM, Madias NE: Diagnosis and Management of Hyponatremia: A Review. *JAMA* [Internet] 328: 280–291, 2022
5. Kheetan M, Ogu I, Shapiro JI, Khitan ZJ: Acute and Chronic Hyponatremia. Front Med (Lausanne). 8: 2021
6. Braconnier A, Vrigneaud L, Bertocchio JP: Hyponatremias: From pathophysiology to treatments. Review for clinicians. *Nephrologie et Therapeutique* 11: 201–212, 2015
7. Jovanovich AJ, Berl T: Where vaptans do and do not fit in the treatment of hyponatremia. Kidney Int. 83: 563–567, 2013
8. Gross PA, Wagner A, Decaux G: Vaptans are not the mainstay of treatment in hyponatremia: Perhaps not yet. Kidney Int. 80: 594–600, 2011
9. Rinschen MM, Schermer B, Benzing T: Vasopressin-2 receptor signaling and autosomal dominant polycystic kidney disease: from bench to bedside and back again. *J Am Soc Nephrol* [Internet] 25: 1140–7, 2014
10. Wang X, Gattone V, Harris PC, Torres VE: Effectiveness of vasopressin V2 receptor antagonists OPC-31260 and OPC-41061 on polycystic kidney disease development in the PCK rat. *J Am Soc Nephrol* [Internet] 16: 846–51, 2005
11. Torres VE, Gansevoort RT, Perrone RD, Chapman AB, Ouyang J, Lee J, et al.: Tolvaptan in ADPKD Patients With Very Low Kidney Function. *Kidney Int Rep* [Internet] 6: 2171–2178, 2021
12. Torres VE, Chapman AB, Devuyst O, Gansevoort RT, Grantham JJ, Higashihara E, et al.: Tolvaptan in patients with autosomal dominant polycystic kidney disease. *N Engl J Med* 367: 2407–18, 2012
13. Gattone VH, Wang X, Harris PC, Torres VE: Inhibition of renal cystic disease development and progression by a vasopressin V2 receptor antagonist. *Nat Med* [Internet] 9: 1323–1326, 2003
14. Greenberg A, Verbalis JG, Amin AN, Burst VR, Chiodo JA, Chiong JR, et al.: Current treatment practice and outcomes. Report of the hyponatremia registry. *Kidney Int* 88: 167–177, 2015
15. Humayun MA, Cranston IC: In-patient Tolvaptan use in SIADH: care audit, therapy observation and outcome analysis. *BMC Endocr Disord* [Internet] 17: 69, 2017
16. Workeneh BT, Jhaveri KD, Rondon-Berrios H: Hyponatremia in the cancer patient. Kidney Int. 98: 870–882, 2020
17. Bilgetekin I, Erturk I, Basal FB, Karacin C, Karadurmus N, Oksuzoglu B, et al.: Tolvaptan treatment in hyponatremia due to the syndrome of inappropriate secretion of antidiuretic

hormone (SIADH): effects on survival in patients with cancer. *Int Urol Nephrol* [Internet] 53: 301–307, 2021
18. Kawada T: Survival analysis in cancer patients with hyponatremia: effectiveness of tolvaptan treatment. *Int Urol Nephrol* 2022
19. Shchekochikhin DY, Schrier RW, Lindenfeld J, Price LL, Jaber BL, Madias NE: Outcome differences in community- Versus hospital- Acquired hyponatremia in patients with a diagnosis of heart failure. *Circ Heart Fail* 6: 379–386, 2013
20. Urbach J, Goldsmith SR: Vasopressin antagonism in heart failure: a review of the hemodynamic studies and major clinical trials. Ther Adv Cardiovasc Dis. 15: 2021
21. Gheorghiade M, Rossi JS, Cotts W, Shin DD, Hellkamp AS, Piña IL, et al.: Characterization and prognostic value of persistent hyponatremia in patients with severe heart failure in the ESCAPE Trial. *Arch Intern Med* 167: 1998–2005, 2007
22. Shams E, Bonnice S, Mayrovitz HN: Diuretic Resistance Associated With Heart Failure. *Cureus* [Internet] 14: e21369, 2022
23. Ellison DH, Felker GM: Diuretic Treatment in Heart Failure. *New England Journal of Medicine* 377: 1964–1975, 2017
24. Gianotti RJ, Cardenas A: Hyponatraemia and cirrhosis. *Gastroenterol Rep (Oxf)* [Internet] 2: 21–6, 2014
JJ, John S, Thuluvath PJ: Hyponatremia in Cirrhosis: An Update. Am J Gastroenterol. 115: 1775–1785, 2020
26. Praharaj DL, Anand AC: Clinical Implications, Evaluation, and Management of Hyponatremia in Cirrhosis. J Clin Exp Hepatol. 12: 575–594, 2022
27. John S, Thuluvath PJ: Hyponatremia in cirrhosis: Pathophysiology and management. World J Gastroenterol. 21: 3197–3205, 2015
28. Habib S, Boyer TD: Vasopressin V2-receptor antagonists in patients with cirrhosis, ascites and hyponatremia. *Therap Adv Gastroenterol* [Internet] 5: 189–97, 2012
29. Yan L, Xie F, Lu J, Ni Q, Shi C, Tang C, et al.: The treatment of vasopressin V2-receptor antagonists in cirrhosis patients with ascites: A meta-analysis of randomized controlled trials. *BMC Gastroenterol* 15: 2015
30. Siqueira F, Kelly T, Saab S: Refractory Ascites: Pathogenesis, Clinical Impact, and Management. *Gastroenterol Hepatol (N Y)* [Internet] 5: 647–656, 2009
31. Salerno F, Guevara M, Bernardi M, Moreau R, Wong F, Angeli P, et al.: Refractory ascites: Pathogenesis, definition and therapy of a severe complication in patients with cirrhosis. Liver International. 30: 937–947, 2010
32. Thuluvath PJ, Alukal JJ, Zhang T: Impact of Hyponatremia on Morbidity, Mortality, and Resource Utilization in Portal Hypertensive Ascites: A Nationwide Analysis. *J Clin Exp Hepatol* 12: 871–875, 2022
33. Corona G, Giuliani C, Parenti G, Norello D, Verbalis JG, Forti G, et al.: Moderate hyponatremia is associated with increased risk of mortality: Evidence from a meta-analysis. *PLoS One* 8: 2013
34. Gheorghiade M, Abraham WT, Albert NM, Gattis Stough W, Greenberg BH, O'Connor CM, et al.: Relationship between admission serum sodium concentration and clinical outcomes in patients hospitalized for heart failure: an analysis from the OPTIMIZE-HF registry. *Eur Heart J* 28: 980–8, 2007
35. Ruf AE, Kremers WK, Chavez LL, Descalzi VI, Podesta LG, Villamil FG: Addition of serum sodium into the MELD score predicts waiting list mortality better than MELD alone. *Liver Transplantation* 11: 336–343, 2005
36. Wald R, Jaber BL, Price LL, Upadhyay A, Madias NE: Impact of hospital-associated hyponatremia on selected outcomes. *Arch Intern Med* 170: 294–302, 2010

37. Corona G, Giuliani C, Parenti G, Colombo GL, Sforza A, Maggi M, et al.: The Economic Burden of Hyponatremia: Systematic Review and Meta-Analysis. *American Journal of Medicine* 129: 823-835.e4, 2016
38. Amin A, Deitelzweig S, Christian R, Friend K, Lin J, Belk K, et al.: Evaluation of incremental healthcare resource burden and readmission rates associated with hospitalized hyponatremic patients in the US. *J Hosp Med* 7: 634–9, 2012
39. Shea AM, Hammill BG, Curtis LH, Szczech LA, Schulman KA: Medical costs of abnormal serum sodium levels. *J Am Soc Nephrol* 19: 764–70, 2008
40. Kinugawa K, Sato N, Inomata T, Yasuda M, Shibasaki Y, Shimakawa T: Novel Risk Score Efficiently Prevents Tolvaptan-Induced Hypernatremic Events in Patients With Heart Failure. *Circulation Journal* [Internet] 82: 1344–1350,
41. Capuano I, Buonanno P, Riccio E, Amicone M, Pisani A: Therapeutic advances in ADPKD: the future awaits. *J Nephrol* [Internet] 35: 397–415, 2022
42. Audrézet M-P, Cornec-Le Gall E, Chen J-M, Redon S, Quéré I, Creff J, et al.: Autosomal dominant polycystic kidney disease: comprehensive mutation analysis of PKD1 and PKD2 in 700 unrelated patients. *Hum Mutat* [Internet] 33: 1239–50, 2012
43. Bergmann C, Guay-Woodford LM, Harris PC, Horie S, Peters DJM, Torres VE: Polycystic kidney disease. *Nat Rev Dis Primers* [Internet] 4: 50, 2018
44. Paul BM, Vanden Heuvel GB: Kidney: polycystic kidney disease. *Wiley Interdiscip Rev Dev Biol* [Internet] 3: 465–87, 2014
45. Weydert C, Decuypere J-P, De Smedt H, Janssens P, Vennekens R, Mekahli D: Fundamental insights into autosomal dominant polycystic kidney disease from human-based cell models. *Pediatr Nephrol* [Internet] 2018
46. Calvet JP: Polycystic kidney disease: primary extracellular matrix abnormality or defective cellular differentiation? *Kidney Int* [Internet] 43: 101–8, 1993
47. Ward CJ, Yuan D, Masyuk T V., Wang X, Punyashthiti R, Whelan S, et al.: Cellular and subcellular localization of the ARPKD protein; fibrocystin is expressed on primary cilia. *Hum Mol Genet* 12: 2703–2710, 2003
48. Mangoo-Karim R, Uchic ME, Grant M, Shumate W a, Calvet JP, Park CH, et al.: Renal epithelial fluid secretion and cyst growth: the role of cyclic AMP. *The FASEB journal : official publication of the Federation of American Societies for Experimental Biology* 3: 2629–2632, 1989
49. Belibi FA, Reif G, Wallace DP, Yamaguchi T, Olsen L, Li H, et al.: Cyclic AMP promotes growth and secretion in human polycystic kidney epithelial cells. *Kidney Int* [Internet] 66: 964–73, 2004
50. Sussman CR, Wang X, Chebib FT, Torres VE: Modulation of polycystic kidney disease by G-protein coupled receptors and cyclic AMP signaling. *Cell Signal* [Internet] 72: 109649, 2020
51. Perrone RD, Oberdhan D, Ouyang J, Bichet DG, Budde K, Chapman AB, et al.: OVERTURE: A Worldwide, Prospective, Observational Study of Disease Characteristics in Patients With ADPKD. *Kidney Int Rep* 8: 989–1001, 2023
52. Zhou X, Davenport E, Ouyang J, Hoke ME, Garbinsky D, Agarwal I, et al.: Pooled Data Analysis of the Long-Term Treatment Effects of Tolvaptan in ADPKD. *Kidney Int Rep* 7: 1037–1048, 2022
53. Lu J, Xu W, Gong L, Xu M, Tang W, Jiang W, et al.: Efficacy and safety of tolvaptan versus placebo in the treatment of patients with autosomal dominant polycystic kidney disease: a meta-analysis. *Int Urol Nephrol* [Internet] 55: 631–640, 2023
54. Anderegg MA, Dhayat NA, Sommer G, Semmo M, Huynh-Do U, Vogt B, et al.: Quality of Life in Autosomal Dominant Polycystic Kidney Disease Patients Treated With Tolvaptan. *Kidney Med* [Internet] 2: 162–171, 2020

55. Joly D, Quinn J, Mokiou S, O'Reilly K, Sánchez-Covisa J, Wang-Silvanto J, et al.: Rationale and study protocol of ACQUIRE, a prospective, observational study measuring quality of life, treatment preference and treatment satisfaction of autosomal dominant polycystic kidney disease (ADPKD) patients in Europe. *BMC Nephrol* 21: 1–10, 2020
56. Müller R-U, Messchendorp AL, Birn H, Capasso G, Cornec-Le Gall E, Devuyst O, et al.: An update on the use of tolvaptan for autosomal dominant polycystic kidney disease: consensus statement on behalf of the ERA Working Group on Inherited Kidney Disorders, the European Rare Kidney Disease Reference Network and Polycystic Kidney Disease International. *Nephrol Dial Transplant* [Internet] 37: 825–839, 2022
57. Gansevoort RT, Arici M, Benzing T, Birn H, Capasso G, Covic A, et al.: Recommendations for the use of tolvaptan in autosomal dominant polycystic kidney disease: a position statement on behalf of the ERA-EDTA Working Groups on Inherited Kidney Disorders and European Renal Best Practice. *Nephrol Dial Transplant* [Internet] 31: 337–48, 2016
58. Clark GC, Casewell NR, Elliott CT, Harvey AL, Jamieson AG, Strong PN, et al.: Friends or Foes? Emerging Impacts of Biological Toxins. *Trends Biochem Sci* [Internet] 44: 365–379, 2019
59. Zambelli VO, Pasqualoto KFM, Picolo G, Chudzinski-Tavassi AM, Cury Y: Harnessing the knowledge of animal toxins to generate drugs. *Pharmacol Res* [Internet] 112: 30–36, 2016
60. Zhang Y: Why do we study animal toxins? *Dongwuxue Yanjiu* 36: 183–222, 2015
61. Harvey AL: Toxins and drug discovery. *Toxicon* [Internet] 92: 193–200, 2014
62. Van Baelen A-C, Robin P, Kessler P, Maïga A, Gilles N, Servent D: Structural and Functional Diversity of Animal Toxins Interacting With GPCRs. *Front Mol Biosci* [Internet] 9: 811365, 2022
63. Ciolek J, Reinfrank H, Quinton L, Viengchareun S, Stura EA, Vera L, et al.: Green mamba peptide targets type-2 vasopressin receptor against polycystic kidney disease. *Proc Natl Acad Sci U S A* [Internet] 114: 7154–7159, 2017
64. Droctové L, Ciolek J, Mendre C, Chorfa A, Huerta P, Carvalho C, et al.: A new Kunitz-type snake toxin family associated with an original mode of interaction with the vasopressin 2 receptor. *Br J Pharmacol* [Internet] 179: 3470–3481, 2022
65. Jensen KK, Andreatta M, Marcatili P, Buus S, Greenbaum JA, Yan Z, et al.: Improved methods for predicting peptide binding affinity to MHC class II molecules. *Immunology* 154: 394–406, 2018
66. Azam A, Gallais Y, Mallart S, Illiano S, Duclos O, Prades C, et al.: Healthy Donors Exhibit a CD4 T Cell Repertoire Specific to the Immunogenic Human Hormone H2-Relaxin before Injection. *The Journal of Immunology* 202: 3507–3513, 2019
67. Droctové L, Lancien M, Tran VL, Susset M, Jego B, Theodoro F, et al.: A snake toxin as a theranostic agent for the type 2 vasopressin receptor. *Theranostics* [Internet] 10: 11580–11594, 2020
68. Cao X, Wang P, Yuan H, Zhang H, He Y, Fu K, et al.: Benzodiazepine Derivatives as Potent Vasopressin V2 Receptor Antagonists for the Treatment of Autosomal Dominant Kidney Disease. *J Med Chem* [Internet] 65: 9295–9311, 2022
69. Zhang H, Yan W, Sun Y, Yuan H, Su L, Cao X, et al.: Long Residence Time at the Vasopressin V_2 Receptor Translates into Superior Inhibitory Effects in *Ex Vivo* and *In Vivo* Models of Autosomal Dominant Polycystic Kidney Disease. *J Med Chem* [Internet] acs.jmedchem.2c00011, 2022
70. Su L, Liu L, Jia Y, Lei L, Liu J, Zhu S, et al.: Ganoderma triterpenes retard renal cyst development by downregulating Ras/MAPK signaling and promoting cell differentiation. *Kidney Int* 92: 1404–1418, 2017
71. Yin L, Chen X, Vicini P, Rup B, Hickling TP: Therapeutic outcomes, assessments, risk factors and mitigation efforts of immunogenicity of therapeutic protein products. 295: 118–126, 2015

72. Delluc S, Ravot G, Maillere B: Quantification of the preexisting CD4 T-cell repertoire specific for human erythropoietin reveals its immunogenicity potential. *Blood* 116: 2010
73. Delluc S, Ravot G, Maillere B: Quantitative analysis of the CD4 T-cell repertoire specific to therapeutic antibodies in healthy donors. *The FASEB Journal* 25: 2040–2048, 2011
74. Sivelle C, Sierocki R, Lesparre Y, Lomet A, Quintilio W, Dubois S, et al.: Combining deep mutational scanning to heatmap of HLA class II binding of immunogenic sequences to preserve functionality and mitigate predicted immunogenicity. *Front Immunol* [Internet] 14: 1197919, 2023
75. Imura R, Ida H, Sasaki I, Ishioka NS, Watanabe S: Re-Evaluations of Zr-DFO complex coordination chemistry for the estimation of radiochemical yields and chelator-to-antibody ratios of ^{89}Zr Immune-PET tracers. *Molecules* 26: 2021
76. Alnahwi AH, Ait-Mohand S, Dumulon-Perreault V, Dory YL, Guérin B: Promising Performance of 4HMS, a New Zirconium-89 Octadendate Chelator. *ACS Omega* 5: 10731–10739, 2020
77. Nair A, Jacob S: A simple practice guide for dose conversion between animals and human. *J Basic Clin Pharm* 7: 27, 2016
78. Miyazaki T, Yamamura Y, Onogawa T, Nakamura S, Kinoshita S, Nakayama S, et al.: Therapeutic effects of tolvaptan, a potent, selective nonpeptide vasopressin V2 receptor antagonist, in rats with acute and chronic severe hyponatremia. *Endocrinology* 146: 3037–3043, 2005
79. Wada K, Matsukawa U, Fujimori A, Arai Y, Sudoh K, Sasamata M, et al.: A novel vasopressin dual V1A/V2 receptor antagonist, conivaptan hydrochloride, improves hyponatremia in rats with syndrome of inappropriate secretion of antidiuretic hormone (SIADH). *Biol Pharm Bull* [Internet] 30: 91–5, 2007
80. Sadick M, Attenberger U, Kraenzlin B, Kayed H, Schoenberg SO, Gretz N, et al.: Two non-invasive GFR-estimation methods in rat models of polycystic kidney disease: 3.0 Tesla dynamic contrast-enhanced MRI and optical imaging. *Nephrol Dial Transplant* 26: 3101–3108, 2011
81. Davies B, Morris T: Physiological parameters in laboratory animals and humans. *Pharm Res* [Internet] 10: 1093–5, 1993
82. Slizgi JR, Lu Y, Brouwer KR, St. Claire RL, Freeman KM, Pan M, et al.: Inhibition of human hepatic bile acid transporters by Tolvaptan and metabolites: Contributing factors to drug-induced liver injury? *Toxicological Sciences* 149: 237–250, 2016
83. Snell DM, Bartley C: Osmotic demyelination syndrome following rapid correction of hyponatraemia. *Anaesthesia* 63: 92–5, 2008
84. Saunders I, Williams DM, Ruslan AM, Min T: Osmotic demyelination syndrome following slow correction of hyponatraemia. *BMJ Case Rep* 14: 2021
85. Dellabarca C, Servilla KS, Hart B, Murata GH, Tzamaloukas AH: Osmotic myelinolysis following chronic hyponatremia corrected at an overall rate consistent with current recommendations. *Int Urol Nephrol* 37: 171–3, 2005
86. Newman DJ, Cragg GM: Natural Products as Sources of New Drugs from 1981 to 2014. *J Nat Prod* 79: 629–661, 2016
87. Sanhajariya S, Duffull SB, Isbister GK: Pharmacokinetics of Snake Venom. *Toxins (Basel)* [Internet] 10: 2018

FIGURE LEGENDS

Figure 1. Human CD4 T cell response to MQ1 and design of MQ1 variants with mitigation of T-cell epitope and enhanced binding activity for human V2R. (A) Sequences of the overlapping 15-mer peptides. Main anchor residues predicted from NetMHC3.2 were highlighted in red. (B) T cell epitope mapping was established by testing the recognition of individual peptides by T cell lines raised against MQ1. (C) Design of MQ1 variants. F4G, T27D, I48E in blue. K39A in green. K_i for human V2R. Score of HLA class II binding of the variants was calculated for high and low affinity by the number of peptides with a percentile respectively below 10% and 20% using NetMHC3.2.

Figure 2. MQ232 pharmacological characterization (A) Competitive binding inhibition of ^{3}H-AVP (1 nM) on human (full lines, stable CHO-hV2R cell line) and rat (dashed line, expressed in transfected HEK) V2R by MQ1 (red), MQ232 (blue) and [^{91}Zr]Zr-DFO-MQ232 (green), n = 5. (B-E) Arunlakshana–Schild plots plotted as mean ± SEM. mBU, milliBRET unit corresponding to the competitive inhibition by MQ1 (red) and MQ232 (blue) of AVP-induced (B) cAMP production in stable CHO-hV2R cell line, n = 3, p = 0.052 (C) β-arrestin-1 recruitment by BRET of β-arrestin-1–YFP and human V2R-Rluc in tsA transfected cell line, n = 4, p = 0.004 (D) internalization of the Flag-Snap human V2R in HEK Magic transfected cell line, n = 3, p < 0.001 and (E) MAP kinase phosphorylation in stable Myc-hV2R HEK cell line, n = 3, p = 0.048 (Supplemental Figure 2). (F) Rat aquaresis (red) and urine osmolality (blue) over a 24-h period for various doses of MQ232. BW = body weight. n = 6 rats per dose. (G) Rat aquaresis *vs* time with increasing doses of MQ232 (0 to 3,000 nmol/kg BW) s.c. injected in control male rats at time zero, n = 6 rats per dose. Aqueous diuresis was measured over 60 hours. Half times ($t_{1/2}$, h) were calculated when possible, following a non-compartmental analysis. (H) Plasma MQ232 concentrations were determined by mass analysis after i.p. injection of 30 and 300 nmol/kg BW and after i.v. injection of 30 nmol/kg BW in control rats (Supplemental Figure 6-8). AUCtot = total Area under curve. Vss = extrapolated total volume of distribution. n = 3 rats per group, non-compartmental analysis. (I) Relationship between aquaresis (30 nmol/kg BW s.c.) and plasma MQ232 concentration (30 nmol/kg BW i.p.). n = 3 rats per group.

Figure 3. Biodistribution and pharmacokinetic of MQ232 derived from PET imaging (A) Model of complexation of ^{89}Zr in DFO[75]. (B) iTLC chromatogram of [^{89}Zr]Zr (red) and [^{89}Zr]Zr-DFO-MQ232 (green). (C) Dual PET/CT imaging with Left: Computed Tomography (CT) scan of a healthy mice showing the bone structure (gray scale). Right: PET/CT imaging at 1 h and 4 h post injection of 40 ± 5 µg (4.28 ± 0.18 MBq) of the radiolabeled peptide [^{89}Zr]Zr-DFO-MQ232 i.v. injected in the tail of control mice (n = 6). A strong signal is observed in the kidneys, whereas the liver exhibits minimal residual signal, and there is a low uptake in the gallbladder attributed to restrained hepatic metabolism. It is worth noting that this signal might be overestimated due to transmetalation. The urinary bladder is prominently visible at 4 hours post-injection, highlighting the substantial renal metabolism and excretion of the radiolabeled compound. The presented images showcase a composite of CT (gray scale) and PET (color scale) for enhanced subject visualization. (D) PET-derived biodistribution of [^{89}Zr]Zr-DFO-

MQ232 in the kidneys, gallbladder, colon, liver, blood (image derived input functions using the heart, a large blood pool, which does not express V2R), bone junction and brain using specific volumes of interest at 1 and 4 h post injection. The kidneys (first column in dark red) concentrated more than 60% of the injected radioactivity (E) [^{89}Zr]Zr-DFO-MQ232 blood concentration over time from which the blood half-life of the compound was extracted using a mono exponential model for data fitting. (F) Pharmacokinetic parameters derived from [^{89}Zr]Zr-DFO-MQ232 PET kinetics in blood and kidneys. AUC: area under curve. %ID: % of injected dose.

Figure 4. MQ232's efficacy in experimental rodent models of hyponatremia and PKDs. For each experiment, a minimum number of animals was used to obtain statistically differences between control and treated groups. (A) Male rat model of hyponatremia SIAD. Six to seven weeks rats were infused through an osmotic pump with 10 ng/h of dDAVP inducing a clear hyponatremia in 2 days. Blood samples were taken just before MQ232 i.p. administration (3.1 or 9.6 nmol/kg BW) or tolvaptan p.o. administration (22 µmol/kg BW) indicated by red arrows. *Ex vivo* mouse model of PKD: (B) The isolated kidney harvested at embryonic day 13.5 were treated with 100 µM 8-Br-cAMP to stimulate cyst growth plus saline (vehicle NaCl 0.9%) or 1 µM MQ232 for 6 days. Representative images of embryonic kidneys cultured with vehicle or 1 µM MQ232 at day 0 and 6. (C) Fractional cyst area (i.e., empty white spots) of kidneys on day 6 were counted. Data are presented as mean ± SEM (vehicle-treated group n = 6, MQ232-treated group n = 8). Orthologue male mouse model of ADPKD: (D) The genotype Pkd1$^{flox/flox}$; Ksp-Cre was selected at postnatal day 2 and mice administrated s.c. with MQ232 (1 µmol/kg BW per day) or saline vehicle (NaCl 0.9%) from day 6 to day 12. Representative images at day 12 of hematoxylin/eosin staining kidney sections (lower) and kidney photography (upper) from *Pkd1$^{flox/flox}$*; *Ksp-Cre* mice. (E) Kidney weight (KW) indexes (KW/BW) of *Pkd1$^{flox/flox}$; Ksp-Cre* mice at day 12. Mean ± SEM (n = 6).

A

```
P1  RPSFCNLPVKPGPCN
P2     FCNLPVKPGPCNGFF
P3        LPVKPGPCNGFFSAF
P4           KPGPCNGFFSAFYYS
P5            PCNGFFSAFYYSQKT
P6               GFFSAFYYSQKTNKC
P7                  SAFYYSQKTNKCHSF
P8                     YYSQKTNKCHSFTYG
P9                        QKTNKCHSFTYGGCK
P10                          NKCHSFTYGGCKGNA
P11                             HSFTYGGCKGNANRF
P12                                TYGGCKGNANRFSTI
P13                                   GCKGNANRFSTIEKC
P14                                      GNANRFSTIEKCRRT
P15                                         NRFSTIEKCRRTCVG
```

B

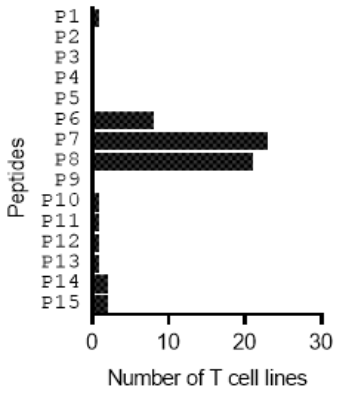

C

	Sequence	K_i nM	HLA-DR binding score High	low
MQ1	RPSFCNLPVKPGPCNGFFSAFYYSQKTNKCHSFTYGGCKGNANRFSTIEKCRRTCVG	4.56	6	11
211	RPSGCNLPVKPGPCNGFFSAFYYSQKTNKCHSFTYGGCKGNANRFSTEEKCRRTCVG	4.30	4	8
228	RPSGCNLPVKPGPCNGFFSAFYYSQKDNKCHSFTYGGCKGNANRFSTEEKCRRTCVG	3.55	0	0
232	RPSGCNLPVKPGPCNGFFSAFYYSQKDNKCHSFTYGGCAGNANRFSTEEKCRRTCVG	0.37	0	0

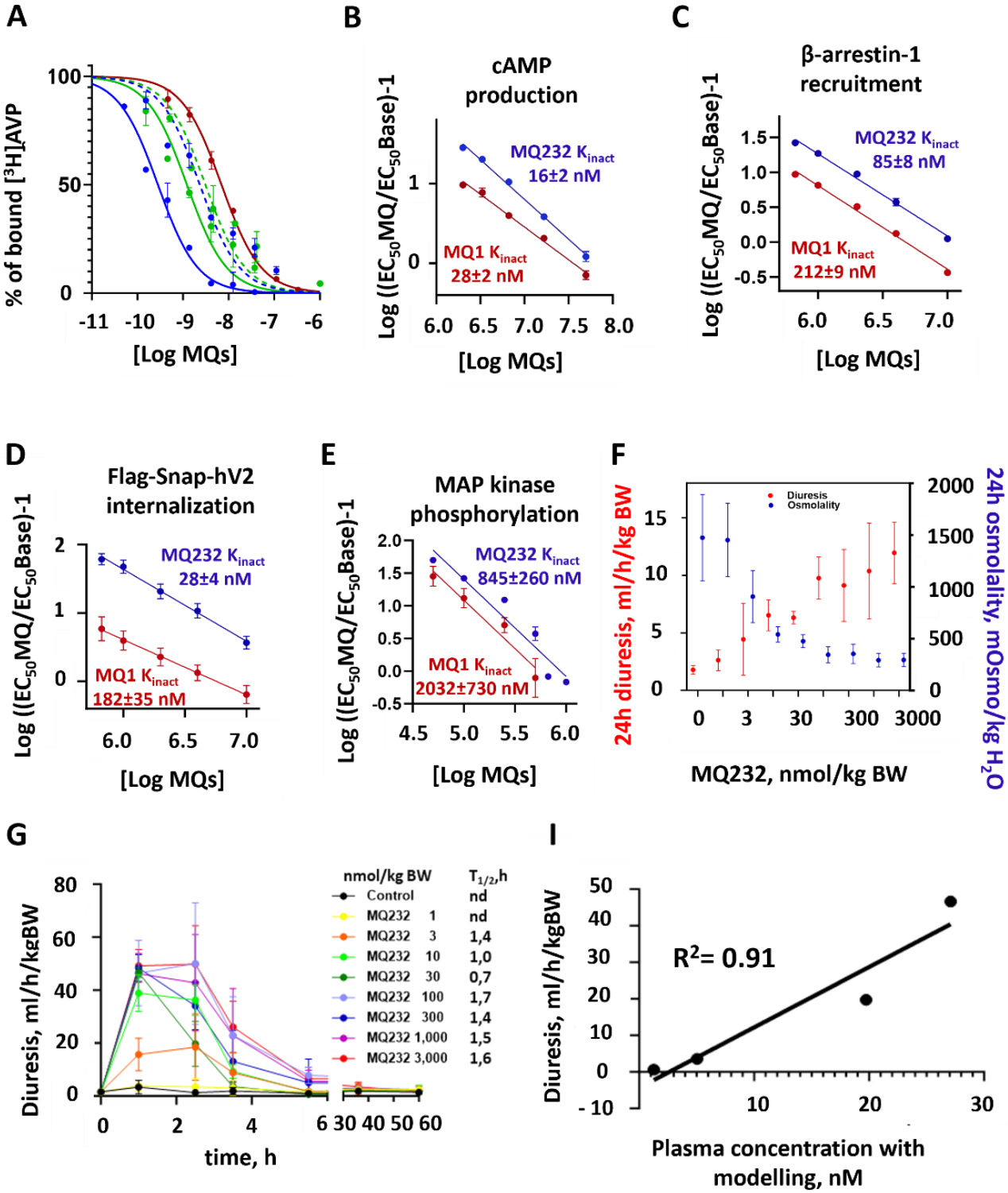

H

Dose nmol/kg	route	AUCtot µg/mL*h	$T_{1/2}$ h	Vss mL/kg	Clearance mL/min/kg
30	i.v.	0.47	0.96	450	7.53
30	i.p.	0.52	1.1	680	6.34
300	i.p.	5.9	2.0	780	7.42

A

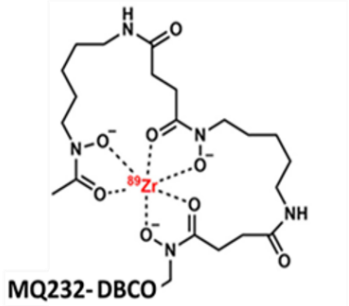

B

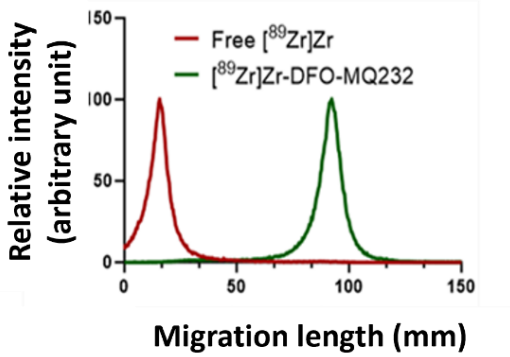

C

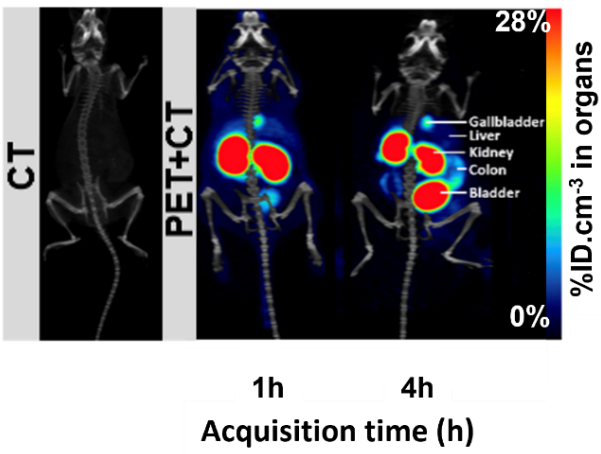

D

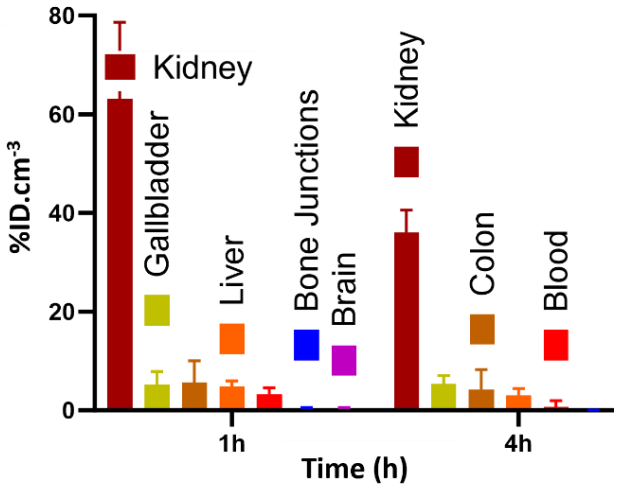

E

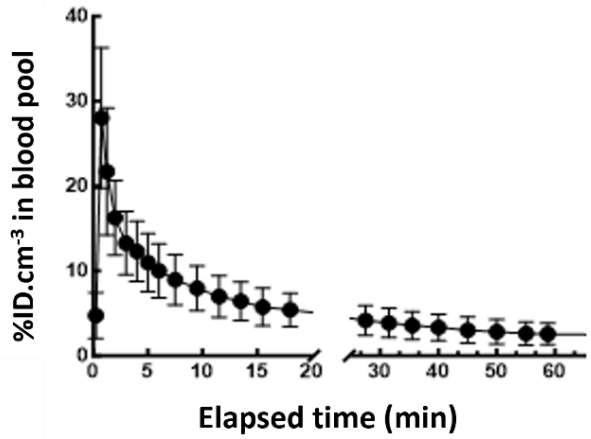

F

$t_{1/2,\ blood}$ (min)	AUC_{blood} (%ID.cm^{-3}.h)	AUC_{kidney} (%ID.cm^{-3}.h)
27 ± 11	10.0 ± 2,1	769 ± 58

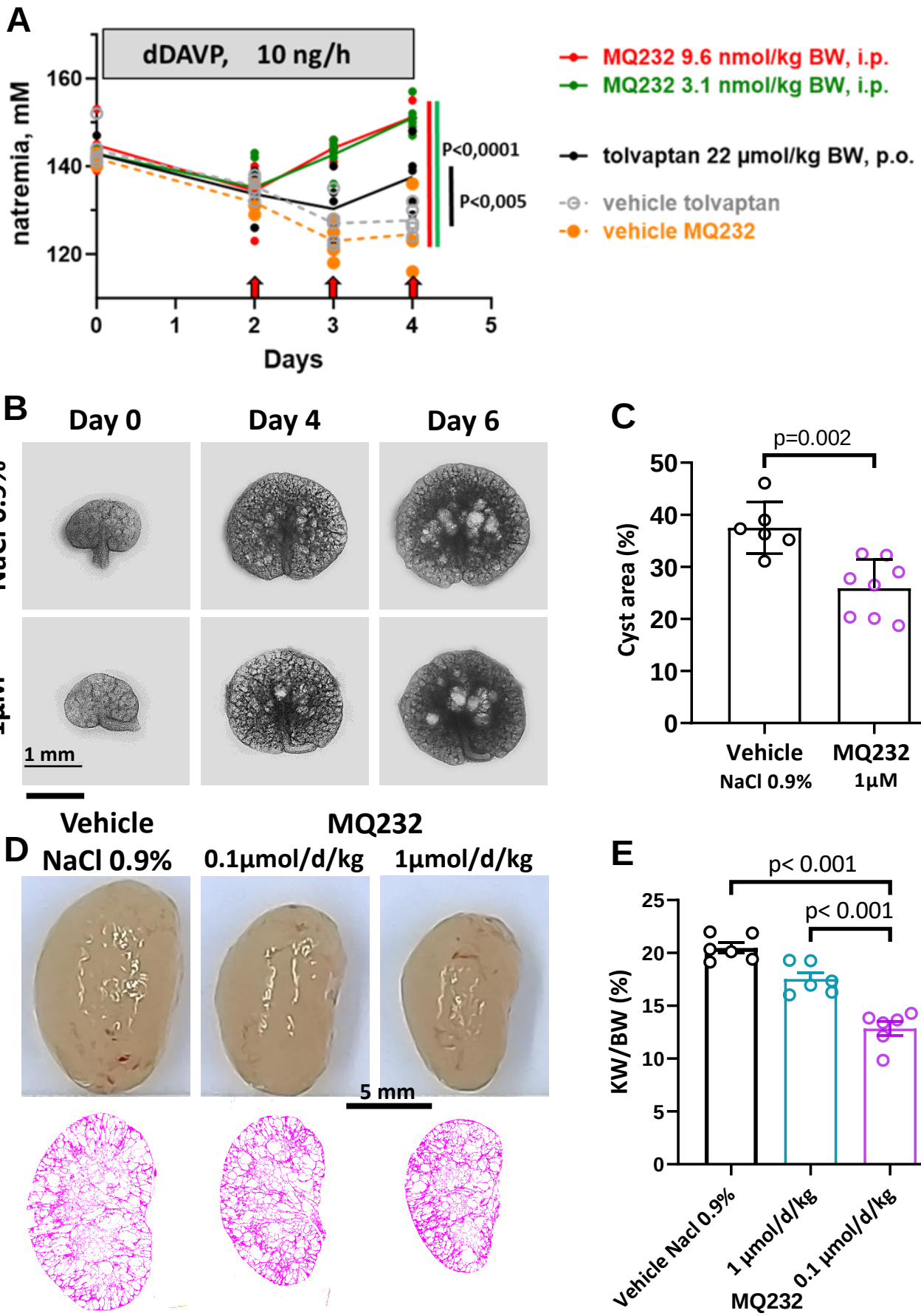
A
dDAVP, 10 ng/h
natremia, mM
160
140
120
0
1
2
3
4
5
Days
P<0,0001
P<0,005
MQ232 9.6 nmol/kg BW, i.p.
MQ232 3.1 nmol/kg BW, i.p.
tolvaptan 22 µmol/kg BW, p.o.
vehicle tolvaptan
vehicle MQ232
B
Day 0
Day 4
Day 6
Vehicle NaCl 0.9%
MQ232 1µM
1 mm
C
p=0.002
Cyst area (%)
50
40
30
20
10
0
Vehicle NaCl 0.9%
MQ232 1µM
D
Vehicle NaCl 0.9%
MQ232 0.1µmol/d/kg
MQ232 1µmol/d/kg
5 mm
E
p< 0.001
p< 0.001
KW/BW (%)
25
20
15
10
5
0
Vehicle Nacl 0.9%
1 µmol/d/kg
0.1 µmol/d/kg
MQ232